J Mater Sci (2010) 45:562–565
DOI 10.1007/s10853-009-4037-z

LETTER

Surface characteristics of 4340 steel treated by electrolytic plasma processing

Y. H. Cheng · P. Gupta · E. I. Meletis

Received: 26 October 2009 / Accepted: 11 November 2009 / Published online: 21 November 2009

Surface cleaning, a crucial pretreatment for coating processes, is routinely used to remove impurities, rust, and mill scale from steel surfaces that inadvertently affect coating adhesion. Traditional surface cleaning techniques such as acid pickling or blasting, suffer from serious environmental problems. Besides these concerns, acid pickling can introduce hydrogen into the material during cleaning, causing premature failure in high-strength steels via hydrogen embrittlement (HE).

Electrolytic plasma processing (EPP) is a newly developed environmentally friendly technique for deep and large scale metal surface cleaning and coating with high efficiency, simplicity, and high process flexibility [1–3]. In this process, an electrical potential is applied between the workpiece (cathode) and a counter electrode (anode) in the presence of an aqueous electrolyte. Above a critical voltage, electrolysis takes place followed by fine hydrogen bubble formation and continuous arcing plasma generation over the entire workpiece surface. High temperatures from the plasma result in localized melting followed by freezing (quenching) at the workpiece surface. Meanwhile, the gaseous vapor plasma can effectively reduce oxide layers and decompose organic hydrocarbon materials present on the workpiece surface. EPP has been shown to be effective in removing surface oxide layers of mill-scale produced by the hot-rolling mill as well as organic materials [3].

Two critical issues relating to applicability of EPP are the effects of the repeated localized melting/quenching cycles on the stress state at the surface and the possibility of hydrogen intake from the generated plasma. Both of these issues are of considerable concern since they can induce HE leading to catastrophic failure of treated high-strength steels.

In the present study, EPP cleaning was conducted on high strength AISI 4340 steel coupons of 24 mm diameter and 1.5 mm thickness. Power density applied to the work piece during processing was $\sim$77.43 W/cm^2. An aqueous electrolyte was used at a temperature of 70 °C. The treatment time was 15 s. All processing was conducted at CAP Technologies (Baton Rouge, Louisiana).

High resolution scanning electron microscopy (SEM) on cross sections of treated 4340 steel specimens was conducted to observe the produced microstructure. Before observation, the specimens were mounted in epoxy, then ground and polished, followed by etching with 2.5% nital reagent. The phase structure, grain size, and internal stress of EPP-treated steel specimens were studied by X-ray diffraction (XRD) using a Siemens D-500 X-ray diffractometer with a CuK_α radiation source. The accelerating voltage and filament current were 40 kV and 30 mA, respectively.

Figure 1 presents a typical cross-sectional SEM image of etched, EPP-treated 4340 steel specimen. A surface layer with a different microstructure of about 2 μm thickness can be clearly distinguished from the bulk. Typical martensite needles with a length of 0.5–10 μm and width of

Y. H. Cheng · E. I. Meletis (✉)
Materials Science and Engineering Department, University of Texas at Arlington, Arlington, TX 76019, USA
e-mail: meletis@uta.edu

P. Gupta
CAP Technologies, Baton Rouge, LA 70820, USA

Present Address:
Y. H. Cheng
American Eagle Instruments, Inc, Missoula, MT, USA

Present Address:
P. Gupta
Boston Scientific, Minneapolis, MN, USA

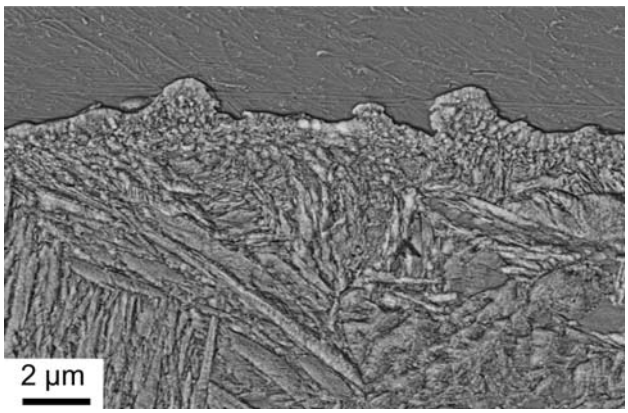

Fig. 1 Typical cross-sectional SEM image of EPC-treated 4340 steel

200–500 nm are present in the bulk. However, the surface layer is composed of a fine grain structure (determined to be nanocrystalline α-Fe as is discussed below). After careful inspection, it was found that the surface layer comprises of two layers: top layer and subsurface layer. The top layer is featureless and amorphous-like, indicating amorphous or nanocrystalline structure. The subsurface layer consists of a fine-grained (about 150 nm) structure. The thickness of the top layer and subsurface layer was about 200–500 nm and 0.5–2 μm, respectively.

The change in the microstructure of the EPP-treated steel by moving away from surface can be understood on the basis of the treatment process. Klapkiv [4] has shown that the temperature inside the electrolytic plasma could rise to 6–7 $\times$ 10^3 K in a millisecond. Subsequently, the workpiece can quench the small molten volume at the surface at a cooling rate of $\sim 10^7$ K/s. This rapid solidification of the small molten volume corresponds to the formation of a non-equilibrium amorphous or nanocrystalline structure. Using high resolution transmission electron microscopy (TEM), we have observed previously the formation of 10 nm grains at the outer surface layer in EPP-treated carbon steel [1]. Actually, the formation of non-equilibrium phases has also been observed in oxide coatings prepared by similar electro plasma processes [5]. Thus, the temperature gradient along the cross section can account for the variation of the grain size in the produced surface layer.

To identify the structure changes in the surface layer produced by the EPP treatment, XRD measurements were conducted in the 2θ range of 20–120° with a θ–2θ scan. XRD patterns show that after the EPP treatment, the crystal structure in the surface layer is mainly composed of BCC α-Fe together with a small amount of martensite, cementite, and retained austenite. As the penetration depth of X-rays with Cu K_α radiation in steel at a glancing angle of 22.5° is only 2 μm [6], the XRD pattern for the EPP-treated steel mostly originates from surface layer.

In order to study the phase structure at different depths, the glancing angle XRD technique was utilized. In this case, the penetration depth of X-ray diminishes with decreasing the angle of incidence. During the measurements, the incidence angle was fixed while the 2θ angle changed from 42 to 47°. It is interesting to see that the (110) diffraction peak becomes broader and shifts to a lower diffraction angle with reducing the glancing angle. Figure 2a presents the peak center position and full width at half maximum (FWHM) of the (110) peak as a function of the glancing angle. With reducing the glancing angle, the (110) peak center position decreases linearly while its FWHM increases linearly with reducing glancing angle down to 1° followed by a rapid increase. The grain size, d, at different glancing angle was computed using the Scherer equation: [6]

$$d = \frac{0.9\lambda}{B\cos\theta}$$

where B is the FWHM of the diffraction peak, and θ is half of the diffraction angle. Meanwhile, the penetration depth (D_θ) of X-rays at different glancing angle (α) can be calculated by the expression: $D_\theta = 2\sin(\alpha)/\sin(22.5)$.

The grain size at different depth is plotted in Fig. 2b. Two distinct regions are shown: a top layer and subsurface

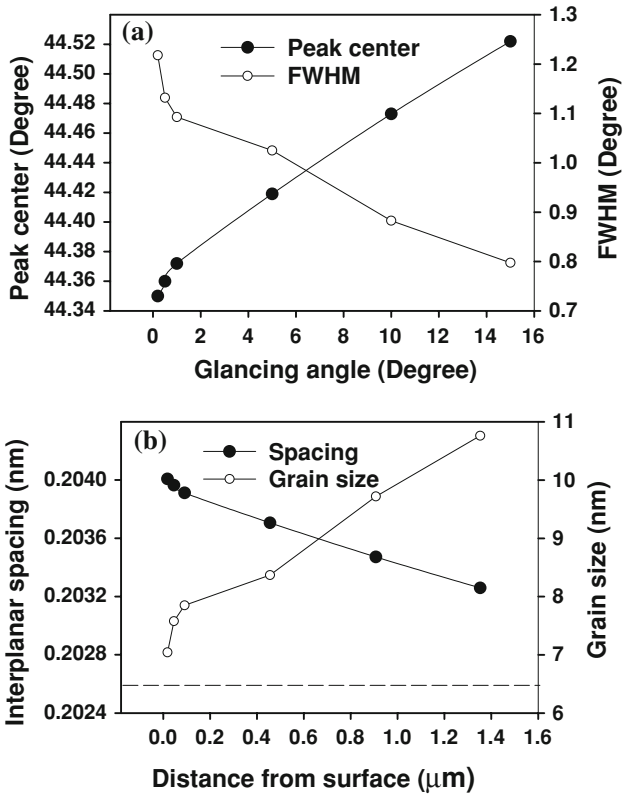

Fig. 2 **a** Dependence of the peak center and FWHM of the XRD peak on the X-ray glancing angle and **b** calculated depth profile of interplanar spacing and grain size

layer. In the top layer (about 200 nm thick), the grain size is fairly small, but it increases rapidly with increasing depth. In the subsurface region, the grain size increases slowly, but monotonically with increasing depth. This is consistent with the SEM observations. It should be noted that the grain size calculated from the FWHM of the XRD peaks measured at higher glancing angles should be larger than the value shown in Fig. 2 because both the surface region and sub-surface region contribute to the XRD pattern. Cross-sectional TEM is necessary to obtain detailed information on the change of grain size as a function of depth. As discussed above, the ultra-small grain size in the surface region results from the rapid freezing of the local melting produced by the process. Furthermore, the gradual change of the grain size is attributed to the pertaining temperature gradient.

Interplanar spacing was obtained from the positions of the diffraction peaks using Bragg's law. The interplanar distance and grain size at different distance from the surface were calculated and plotted in Fig. 2b. The dotted line in the graph is the interplanar distance of α-Fe obtained from PDF standard files. It can be seen that the interplanar distance decreases linearly with increasing distance from surface. Zhang et al. [7] proposed that the stress, σ, in films can be obtained using glancing angle X-ray diffraction by

$$\sigma = -\frac{E}{v}\Delta l,$$

where $\Delta l = (l - l_0)/l_0$; E and v are the Young's modulus and Poisson's ratio, respectively; l_0 is the distance of the unstressed *hkl* plane, l represents the distance of the stressed *hkl* plane in the direction normal to the sample surface, which is defined as: $l = \frac{d_{hkl}}{\cos(\theta-\alpha)}$, where d_{hkl} is the d-spacing of the diffracted *hkl* plane and α is the X-ray incidence angle. It can be seen from this equation that the larger interplanar spacing in the near surface region indicates the presence of a higher compressive stress, and the decrease of interplanar spacing implies a reduction of compressive stresses with depth. However, it is difficult to calculate the internal stress at different depth since it is hard to determine the value of l_0.

In order to investigate the existence of a compressive stress and obtain qualitative information about the internal stress in the EPP-treated surface layer, the standard $d_{hkl}(\psi)$ versus $\sin^2(\psi)$ method was used. The (310) ferrite reflection was used for the stress measurements due to its high diffraction angle (about 116.4°) and relatively high intensity. During measurement, the specimen surface was tilted 0–30° (ψ angle) and a θ–2θ scan was conducted in the 2θ range of 110–120°. The calculated $(d_\psi - d_0)/d_0$ vs. $\sin^2(\psi)$ is plotted in Fig. 3. As shown, the $(d_\psi - d_0)/d_0$ decreases linearly with increasing $\sin^2(\psi)$, indicating a compressive stress. For cubic structures, the stress (σ) in a thin layer in a state of equi-biaxial stress could be computed according to the $\sin^2(\psi)$ method by the following equation [8]

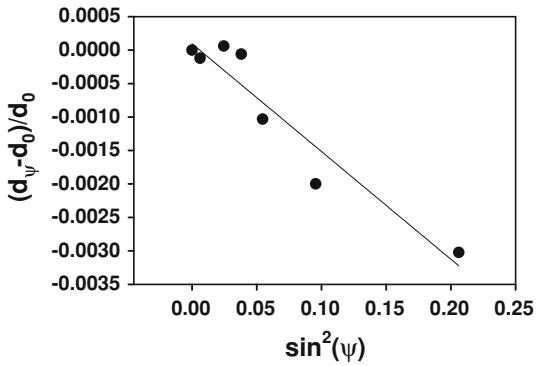

Fig. 3 $(d_\psi\text{-}d_0)/d_0$ vs. $\sin^2(\psi)$ plot for the (310) ferrite reflection

$$\frac{d_{hkl}(\psi) - d_0}{d_0} = \sigma\left[\frac{1+v}{E}\sin^2(\psi) - \frac{2v}{E}\right],$$

where d_0 is the stress-free lattice parameter, $d_{hkl}(\psi)$ is the lattice spacing measured with the surface tilted at ψ angle, v and E are the Poisson's ratio and elastic modulus, which are 0.29 and 200 GPa, respectively for 4340 steel [9]. The internal stress in the surface layer can be calculated from this equation after obtaining the slope of the $(d_\psi - d_0)/d_0$ vs. $\sin^2(\psi)$ plot. The internal stress is calculated to be −1.8 GPa. The negative sign indicates that the stress in the surface layer is compressive. Such high compressive stress at the surface layer is expected to be beneficial to resist crack initiation that may be produced by fatigue or stress environment interaction phenomena (HE, stress corrosion cracking, etc.).

The compressive stress maybe a consequence of the collapsing of hydrogen bubbles formed during EPP treatment, which produces a low-frequency shock wave on the steel surface. The shock wave could generate a compressive stress in the surface layer. It is expected that the amplitude of the shock wave diminishes with increasing distance from steel surface, corresponding to a decrease in internal stress. In addition, during EPP treatment, the voltage is applied to a thin near-electrode plasma region generating a high electric field between 10^6 and 10^8 V/m[5]. The high electric field in the plasma accelerates the anions providing kinetic energy. The bombardment of the surface layer by the energetic ions could also contribute to the observed internal compressive stress. This phenomenon has been widely observed in thin film physical vapor deposition involving ion bombardment [10].

The hydrogen content at the surface region of untreated and EPP-treated 4340 steel was measured using the nuclear reaction analysis (NRA) method. Both specimens exhibit a higher H content at the outer surface, Fig. 4, which is an effect caused by humidity and is typically observed in

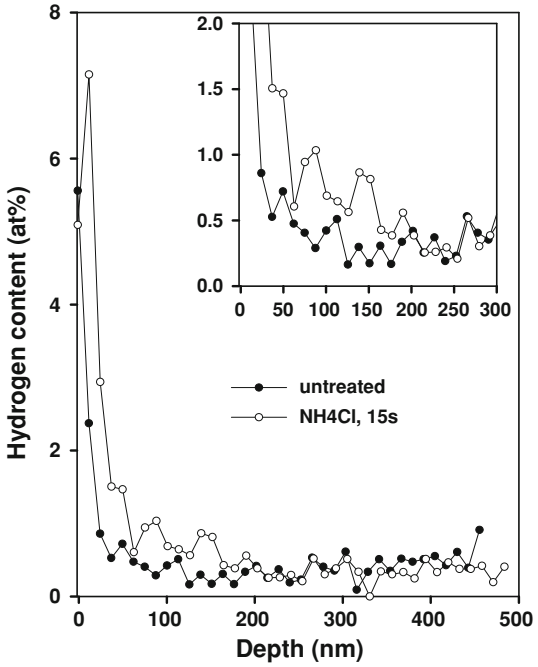

Fig. 4 Depth profile of hydrogen content in untreated and EPP-cleaned 4340 steel

many materials. Compared to the untreated specimen, the H profile of the EPP-treated specimen exhibited a thin layer of about 200 nm with a slightly higher H content ($\sim$0.5 at.%). Beyond that depth, the profiles of untreated and EPP-treated specimens are merely identical. This indicates that only an extremely small amount of H may be trapped in the EPP-treated 4340 steel and is located at the outermost surface region.

HE is a crucial performance characteristic for high-strength steels. In order to investigate the HE susceptibility of the EPP-treated steel, standard HE testing (ASTM-F-519) was conducted. First, untreated C-ring specimens were overloaded mechanically to establish the Notched Fracture Strength (NFS) of the 4340 steel. Then, EPP-treated C-ring specimens were loaded at 75% of the NFS for 200 h (hydrogen sensitivity criterion). All specimens endured the 200 h minimum duration without fracture. In fact, the specimens remained under load for an additional period of 4 months without fracture clearly showing that EPP cleaning does not induce HE susceptibility.

In summary, after treatment with EPP, a surface nanocrystalline layer with a thickness of about 2 μm formed on the 4340 steel surface. The grain size increases with increasing depth. Furthermore, a compressive internal stress exists in the surface layer with higher internal stresses closer to the surface. A small amount of hydrogen was determined by NRA in a shallow depth (200 nm) from the surface. Hydrogen embrittlement testing of EPP-treated 4340 steel showed no susceptibility indicating that EPP can be a suitable technique for cleaning of high-strength steels.

Acknowledgements This work was supported by SERDP (Strategic and Environmental Research and Development Program) Project NOO173-03-2113. The authors thank Drs. Haralabos Efstathiadis (Albany Nanotech Institute) for the Nuclear Reaction Analysis, Scott Grendahl (US Army Research Laboratory) for the hydrogen embrittlement testing and Eddie Daigle (CAP Technologies) for assisting with the electrolytic plasma processing of the samples.

References

1. Meletis EI, Nie X, Wang FL, Jiang JC (2002) Surf Coat Technol 150:246
2. Schilling PJ, Herrington PD, Daigle EO, Meletis EI (2002) J Mater Eng Perform 11:26
3. Gupta P, Tenhundfeld G, Daigle EO, Schilling PJ (2005) Surf Coat Technol 200:1587
4. Klapkiv MD (1995) Mater Sci 31:494
5. Yerokhin AL, Nie X, Leyland A, Matthews A, Dowey SJ (1999) Surf Coat Technol 122:73
6. Cullity BD, Stock SR (2001) Elements of X-ray diffraction. Prentice Hall, Upper Saddle River, NJ, 07458, p 399
7. Zhang S, Xie H, Zeng X, Hing P (1999) Surf Coat Technol 122:219
8. Rafaja D, Valvoda V, Kuzel R, Perry AJ, Treglio JR (1999) Surf Coat Technol 86:302
9. Murr LE, Staudhammer KP, Meyers MA (1995) Metallurgical and materials applications of shock-wave and high-strain-rate phenomena. Elsevier Science, Amsterdam, The Netherlands, p 543
10. Cheng YH, Tay BK (2003) J Vac Sci Technol A 21(5):1609
11. IAW ASTM E8 (Standard test methods for tension testing of metallic materials AASHTO No.: T68 E (2002)